JOURNAL OF MAGNETIC RESONANCE **124,** 343–351 (1997)
ARTICLE NO. MN961018

# The Influence of a Nonconstant Magnetic-Field Gradient on PFG NMR Diffusion Experiments. A Brownian-Dynamics Computer Simulation Study

BJÖRN HÅKANSSON,* BENGT JÖNSSON, PER LINSE, AND OLLE SÖDERMAN

*Division of Physical Chemistry 1, Center for Chemistry and Chemical Engineering, Lund University, P.O. Box 124, S-221 00 Lund, Sweden*

Received May 7, 1996; revised September 26, 1996

**The influence of a nonconstant magnetic-field gradient on the performance of pulsed-field-gradient NMR diffusion experiments was investigated by performing Brownian-dynamics simulations for two different coil designs using two different active sample volumes for each coil. The active sample volumes were chosen in order to represent different degrees of deviation from a perfectly constant magnetic-field gradient. The results show that one can actually tolerate a rather large deviation from a perfectly constant magnetic-field gradient and still obtain accurate values of the self-diffusion coefficients. The dependence of $\Delta$ (the observation time) and the dependence of $D$ (the self-diffusion coefficient) while keeping $D$ and $\Delta$ constant, respectively, were also investigated for three of the active sample volumes. The simulations show that the effects due to a nonconstant field gradient depend only slightly on the values of $\Delta$ and $D$. In conclusion, the Brownian-dynamics computer simulations procedure is a quantitative way of investigating the performance characteristics of a gradient coil of a certain design before it is built.** 

## INTRODUCTION

The determination of self-diffusion coefficients by means of the pulsed-field-gradient (PFG) method is a versatile experiment (*1–3*). In particular, it has been very useful in the field of solution structure of complex fluid systems such as micellar and microemulsion solutions (*4, 5*) and cubic liquid-crystalline phases (*6, 7*). Quite recently, it has also been used to probe structures in porous systems in a fashion similar to scattering experiments (*8, 9*). Characterization of emulsions (*10*), e.g., with respect to their droplet size distribution (*11–14*), is yet another application.

When measuring self-diffusion with the PFG method, one uses essentially a standard NMR probe to which a magnetic-field-gradient coil is added, producing a varying magnetic field (the variation should be linear) superimposed on the main field ($B_0$) of the magnet. The gradient coil that induces the magnetic-field gradient over the active sample volume (the active sample volume is taken to be the volume enclosed by the RF coil) may vary in design due to factors such as available space, required direction of the gradient (i.e., *z*, *x*, or *y*), and desired strength of the gradient. The anti-Helmholtz coil (*15, 16*) (also called the Maxwell pair) and the quadrupole coil (*17–19*) are two common coil configurations used today. There are also other types of configurations reported in the literature (*20–22*). The quadrupole coil has some definite advantages over other configurations. It gives field-gradient uniformity over large sample volumes and has lower inductance. The latter property is important for better performance in high-gradient PFG experiments, since it allows for rapid rise and fall times of the gradient pulses.

However, the quadrupole coil is not a suitable choice when using superconducting magnets. The reasons for this fact is that the direction of the main field is such that the gradient coil must be placed perpendicular to the main field, which is impractical. Therefore the anti-Helmholtz coil is a preferable choice of coil configuration in superconducting magnets.

It is well known (*23, 24*) that a large pulsed gradient produces field disturbances which may persist long after the gradient is switched off. The most effective way of circumventing this problem is to actively shield (*25–27*) the main gradient coil so that the far field will be reduced and gradient shape distortions from eddy currents and other induction-related effects will be diminished. When the gradient coil is shielded, the gradient strength is decreased and the gradient uniformity is often deteriorated over the active sample volume (*28*). Another obvious way of reducing the far field is to place the main gradient coil as close as possible to the sample. Such an arrangement will also increase the gradient strength over the active sample volume, which is favorable when measuring slow diffusion, e.g., high-molecular-weight polymer diffusion. By moving the main gradient coil closer to the sample, the gradient uniformity over the active sample volume also deteriorates. The question is then how these

* To whom correspondence should be addressed.



1090-7807/97 $25.00

deviations from a perfectly constant magnetic-field gradient, which is assumed in the theory relating the echo intensities to the diffusion coefficient, influence the diffusion experiments in practice.

In this paper, we address this question by employing Brownian-dynamics computer simulations. In the investigations we have used two different gradient coil designs. The first one is a gradient coil of our own design optimized over an active sample volume with $r = 5$ mm and $z = \pm 10$ mm and the second one is a gradient coil design taken from the literature (*29*) optimized over an active sample volume with $r = 4$ mm and $z = \pm 4$ mm (see Table 1). For each gradient coil, we have performed simulations for two different active sample volumes, to represent different degrees of deviation.

The disposition of this paper is as follows. First, we give a short theoretical background and some comments concerning the computational details. Subsequently, we discuss the numerical simulation method used. We then present the results from the Browian-dynamics computer simulations. Finally, results from the outcome of a ''practical'' experiment for each coil design and one active sample volume are given. Some comments on the results will also be presented.

## THEORETICAL AND COMPUTATIONAL CONSIDERATIONS

*Introduction.* The simplest version of a PFG NMR experiment (*30*) is based on the pulse sequence shown in Fig. 1. For the case of free diffusion, the echo decay is given by

$$E(\delta, \Delta, g, \tau) = E_0 \exp\left[-\gamma^2 g^2 \delta^2 \left(\Delta - \frac{\delta}{3}\right) D\right], \quad [1]$$

where $E(\delta, \Delta, g, \tau)$ and $E_0$ are the echo intensities at time $2\tau$ in the presence of gradient pulses of strength $g$ and in the absence of any gradient pulses, respectively. The time between the 90° and 180° pulses is $\tau$, $\gamma$ is the gyromagnetic ratio, $\delta$ is the length of the gradient pulses, $\Delta$ is the distance between the leading edges of the gradient pulses, and $D$ is the self-diffusion coefficient. The experiment is usually carried out under conditions of constant $\tau$, which means that the relaxation term [$E_0 = E_{\tau=0}\exp(-2\tau/T_2)$, where $T_2$ is the transverse (spin–spin) relaxation time] is constant and can be omitted. In what follows we will assume that such is the case, and normalize all the intensities by assuming that the term $E_0$ is equal to one, and it is understood that the echo intensity is always estimated at $2\tau$. In the presentation of the data, we will make use of the variable $k$, defined as $k \equiv \gamma^2\delta^2(\Delta - \delta/3)$. Throughout, we will use the value of $\gamma$ for protons (viz. $26.7520 \times 10^7$ rad $T^{-1}s^{-1}$).

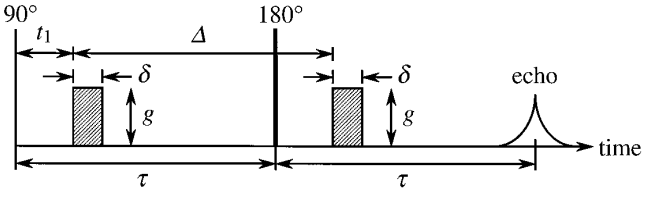


**FIG. 1.** The basic Stejskal–Tanner pulsed-field-gradient experiment (*30*). The symbols are interpreted as follows: $\delta$ is the length of the gradient pulse, $\Delta$ is the distance between the leading edges of the gradient pulses, and $g$ is the gradient strength.

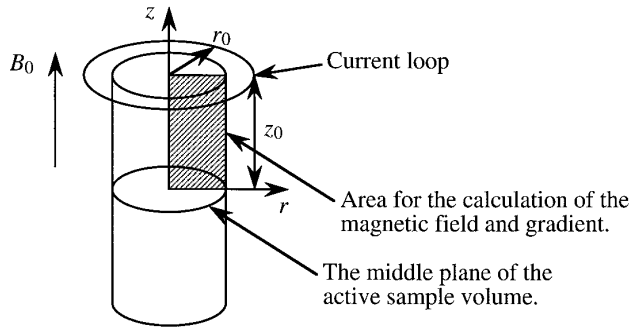


**FIG. 2.** Schematic picture over the active sample volume. The shaded area represents the area over which the calculations are performed. The coordinates used in Eqs. [2]–[4] are also illustrated.

*Magnetic-field and gradient calculations.* In the PFG experiment, it is assumed that the magnetic-field gradient ($g$) is constant over the active sample volume. In reality, this is not the situation, especially when the gradient coil is of the anti-Helmholtz type used in a superconducting magnet (see discussion above).

By knowing the positions of the current loops for the gradient coil, one can calculate the magnetic field [$B_z(r, z)$] and gradient [$dB_z(r, z)/dz$] to obtain their spatial variation. The magnetic field and its gradient at the coordinates $(r, z)$ arising from a current loop at $(r_0, z_0)$ (see Fig. 2) are given by (*31*)

$$B_z(r, z) = \frac{\mu_0 I}{2\pi} \frac{1}{[(r + r_0)^2 + (z - z_0)^2]^{1/2}} \times \left[\frac{r_0^2 - r^2 - (z - z_0)^2}{(r - r_0)^2 + (z - z_0)^2} E(m) + K(m)\right] \quad [2]$$

$$\frac{dB_z(r, z)}{dz} = -\frac{\mu_0 I m^{3/2}(z - z_0)}{16\pi r^{5/2}\sqrt{r_0}} \times \left[\frac{2m - m^2 + (-m^2 + m - 1)(r/r_0)}{(1 - m)^2} E(m) - \frac{0.5m - (1 - 0.5m)(r/r_0)}{1 - m} K(m)\right], \quad [3]$$

where $\mu_0$ is the magnetic permeability for vacuum, $I$ is the current, and $m$ is given by

$$m = \frac{4rr_0}{(r + r_0)^2 + (z - z_0)^2}. \quad [4]$$

$K(m)$ and $E(m)$ represent complete elliptic integrals of the first and second kind, respectively (*32*). With these equations, and by assuming linear superposition, the magnetic field and gradient are obtained by summing over all current loops.

It is impractical to use Eqs. [2] and [4] in the simulations, since the computation time of the magnetic-field strength from these equations will be considerable. Therefore, $B_z$ was represented by a polynomial according to

$$B_z(r, z) = P_1 + P_2 r + P_3 z + P_4 r^2 + P_5 z^2 + P_6 r^3 + P_7 z^3 + P_8 rz + P_9 r^2 z + P_{10} r z^2, \quad [5]$$

where $r$ and $z$ are the coordinates in space as defined in Fig. 2, and $P_n$ are expansion coefficients. The current was assumed to occur in the center of the wires as given by the coordinates of the loops. Polynomial expansions of the elliptic integrals in Eqs. [2] and [3] were used (*32*). For reasons of symmetry, the calculations were performed only over the area that is shown by Fig. 2, and between 66 and 81 calculation points were used for the four active sample volumes. The accuracy of the fits of Eq. [5] to the points generated by Eqs. [2] and [4] is in general quite reasonable. Figure 3 shows one typical $B_z$ field and the difference between the polynomial representation and the ''exact'' field is also included. For reference, we have summarized the coil characteristics in Table 1 for each coil design and the four different active volumes. Finally, we note that the sensitivity of the signal detected depends on the position in the RF coil. In what follows, we have ignored this fact and assume that each volume element in the active sample volume contributes equally to the signal.

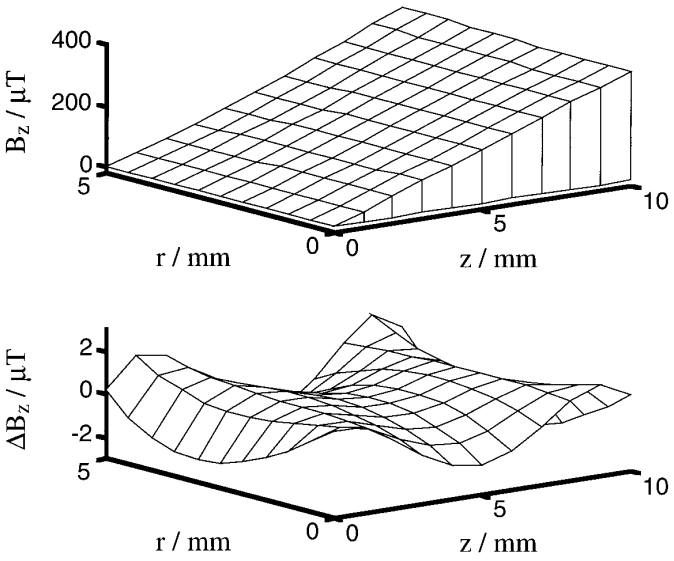


**FIG. 3.** A typical fit of Eq. [5] to $B_z$ calculated according to Eqs. [2] and [4] (upper panel). Also shown are the differences between the fit and the calculated values (lower panel). The calculations were performed for the coil configuration A (see Table 1).

**TABLE 1**
**Coil Characteristics for the Two Coil Designs and the Four Active Sample Volumes Investigated**

| Coil | Active sample volume: $r_{max}$ (mm)[b] | Active sample volume: $z_{min,max}$ (mm)[b] | Mean gradient[a] (mT m$^{-1}$) | Figure |
|---|---|---|---|---|
| A[c] | 5 | ±10 | 36.09 | 4a |
| B[c] | 2.5 | ±5 | 34.48 | 4b |
| C[d] | 5 | ±10 | 33.33 | 4c |
| D[d] | 4 | ±4 | 36.30 | 4d |

[a] Calculated over the active sample volume, using Eqs. [3] and [4]. The mean gradient was obtained from 40,401 calculation points.
[b] See Fig. 2.
[c] Coil design of our own.
[d] Coil design by Gibbs *et al.* (*29*).

*Gradient surfaces.* Figure 4 shows the four gradient surfaces evaluated from Eqs. [3] and [4]. The results in the contour plots are the relative deviations ($100 \times [(g - g_{mean})/g_{mean}]$) from the mean gradient over the active sample volume (see Table 1). The largest deviation for the best case is approximately 4% (D) and for the worst case, approximately 50% (C). The large deviation in the second case is explained by the fact that the coil is not optimized over such a large active sample volume. Nevertheless, the result from C is included for comparison.

## COMPUTER SIMULATIONS

The use of Brownian-dynamics computer simulations is a simple way of investigating how deviations from a perfectly constant gradient influence the attenuation of the signal. The outcome of the simulations will be exact (for a given field-gradient profile) and suffer only from statistical uncertainty. However, by increasing the length of the simulation, one may obtain data with any desired accuracy.

The algorithm for generating the motion of a single molecule in the space[1] of the active sample volume is given by

[1] It should be remarked that in order to restrict the Brownian motion to the configurational space only, the time step $\Delta t$ must be larger than the relaxation time of the velocity–time correlation function. For small molecules such as water, the relaxation time is on the order of picoseconds and since $\Delta t$ used is on the order of milliseconds, the condition is well fulfilled.

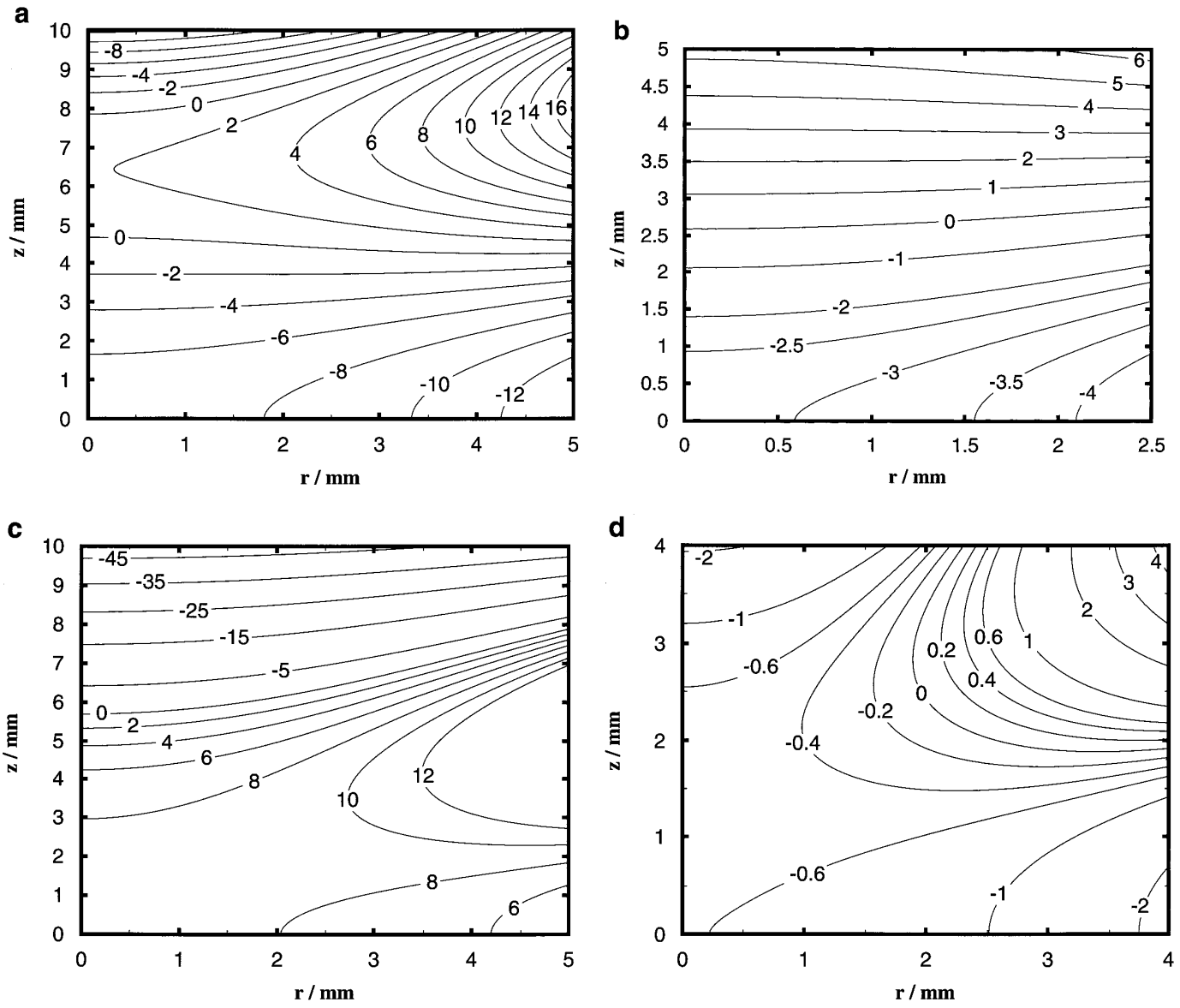


**FIG. 4.** Relative deviations (in %) from the mean gradient (see Table 1) over the active sample volume for case (a) A, (b) B, (c) C, and (d) D.

$$\mathbf{r}(t + \Delta t) = \mathbf{r}(t) + \mathbf{R}(\Delta t), \quad [6]$$

where $\mathbf{r}(t)$ is the position of the molecule at time $t$, $\mathbf{r}(t + \Delta t)$ is the position at a time interval $\Delta t$ later, and $\mathbf{R}(\Delta t)$ is a random displacement vector representing the result of the collisions of the molecule with its surroundings during $\Delta t$ (*33*, *34*). The components of $\mathbf{R}(\Delta t)$ were taken from a Gaussian probability distribution function with the statistical properties

$$\langle \mathbf{R}_\alpha(\Delta t) \rangle = 0 \quad [7]$$

$$\langle \mathbf{R}_\alpha(\Delta t) \cdot \mathbf{R}_\beta(\Delta t) \rangle = 2D\Delta t \delta_{\alpha\beta}, \quad [8]$$

where $D$ is the self-diffusion coefficient of the molecule, and $\delta_{\alpha\beta}$ is the Kronecker delta symbol. The starting position was randomly selected from a homogeneous density distribution in the active volume.

The simulated phase shift $\phi$ of molecule $i$ is, for the pulse sequence in Fig. 1, given by

$$\phi_i[\delta, \Delta, B_z(r, z)] = \gamma B_0 t + \Delta\phi_i, \quad [9]$$

where the first term describes the Larmor precession due to the main field of the magnet. This term is constant over the active sample volume and can be omitted. The simulated

phase shift $\Delta\phi_i$ caused by the diffusion of molecule $i$ can be written as

$$\Delta\phi_i[\delta, \Delta, B_z(r, z)] = \gamma\left[\int_{t_1}^{t_1+\delta} B_z[r_i(t), z_i(t)]dt - \int_{t_1+\Delta}^{t_1+\Delta+\delta} B_z[r_i(t), z_i(t)]dt\right] \approx \gamma\left[\sum_{j=t_1}^{t_1+\delta} B_z(r_{i,j}, z_{i,j}) - \sum_{j=t_1+\Delta}^{t_1+\Delta+\delta} B_z(r_{i,j}, z_{i,j})\right](\Delta t), \quad [10]$$

where $B_z(r, z)$ is described by Eq. [5] and $t_1$ is the time of the application of the first gradient pulse (see Fig. 1). The other quantities are given elsewhere. For a given set of system parameters $\gamma$, $B_z(r, z)$, $\delta$, and $\Delta$, the distribution of the phase shift $P(\Delta\phi)$ was obtained by simulating $N$ spin trajectories. Finally, the attenuation of the spin echo due to the diffusion was calculated from

$$E[\delta, \Delta, B_z(r, z)] = \int_{-\infty}^{\infty} P(\Delta\phi)\cos(\Delta\phi)d(\Delta\phi) \approx \frac{1}{N}\sum_{i=1}^{N} \cos(\Delta\phi_i), \quad [11]$$

where all the symbols are defined above. An attenuation curve corresponding to several $\delta$ values was sampled for each trajectory.

The uncertainty of the simulated attenuation is given as one standard deviation. It is estimated from the spread of subbatches of the total number of trajectories according to

$$\sigma^2(\langle E\rangle) = \frac{1}{n_b(n_b - 1)}\sum_{b=1}^{n_b} (\langle E\rangle_b - \langle E\rangle)^2, \quad [12]$$

where $\langle E\rangle_b$ is the attenuation from one subbatch consisting of $N/n_b$ trajectories, $\langle E\rangle$ is the attenuation from the $N$ trajectories, and $n_b = 10$ is the number of subbatches.

In order to verify the numerical procedure, simulations were first carried out in the case of constant $g$. Figure 5 shows the simulated attenuation vs $k$. The simulated results were obtained by using $N = 10^5$ trajectories and a time step $\Delta t = 0.01$ ms. The estimated standard deviation of the attenuation according to Eq. [12] is in the range of 0.000 to 0.0015 with a mean of 0.0009. Also shown in Fig. 5 is a fit of Eq. [1] to the simulated data, and the difference between the simulated data and the fit for each $k$ value. The difference is at most 0.0005. Thus, this verifies the simulation procedure and indicates that the error in the simulated attenuation is well within the estimated standard deviation. The residuals are not randomly distributed since attenuations for all $\delta$ values were collected for each trajectory (see discussion below). If not stated otherwise, the same simulation parameters were used, viz. $N = 10^5$ trajectories and a time step $\Delta t$ of 0.01 ms, for all subsequent simulations. Under these conditions, the CPU time required for a single simulation covering different $\delta$ values was at most 12 hours on an IBM RS/6000 590 workstation.

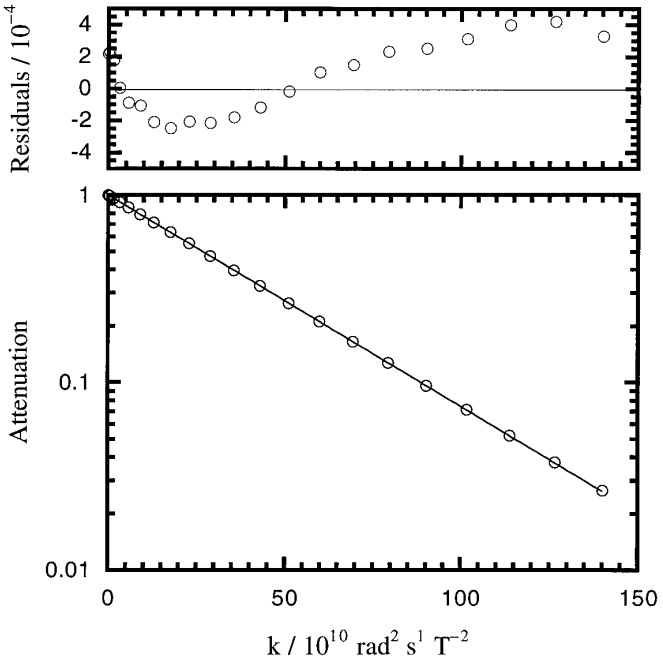


**FIG. 5.** Attenuation (○) vs $k$ [$k \equiv \gamma^2\delta^2(\Delta - \delta/3)$] from the simulation of free diffusion with constant $g$. A nonlinear least-squares fit of Eq. [1] to the data is included (—) as well as the residuals (○) between the simulation and the fit. Parameters used: $\Delta = 140$ ms, $D = 2 \times 10^{-9}$ m$^2$s$^{-1}$, and $g = 0.036$ T m$^{-1}$.

## RESULTS AND DISCUSSION

This section contains two parts. First, we will discuss the results of the computer simulations. Then we present results of a ''practical'' experiment, in which the common protocol for determining self-diffusion coefficients in a real experimental situation has been followed.

*Simulations.* In Fig. 6 the results of the computer simulations for the four active sample volumes are shown. Results from a nonlinear least-squares fit of Eq. [1] to the data, where $g$ and the physically irrelevant parameter $E_0$ (see Eq. [1]) are optimized, are also included, as well as the residuals between the fit and the simulated points. The residuals in Fig. 6 are considerably larger (by a factor of 20 for the ''worst'' case) than those in Fig. 5. The increased values of the residuals are caused by the fact that we are now fitting an equation which is strictly only valid for the case of a constant field gradient to data where this is clearly not the case. Thus, the difference in magnitude of the residuals be-

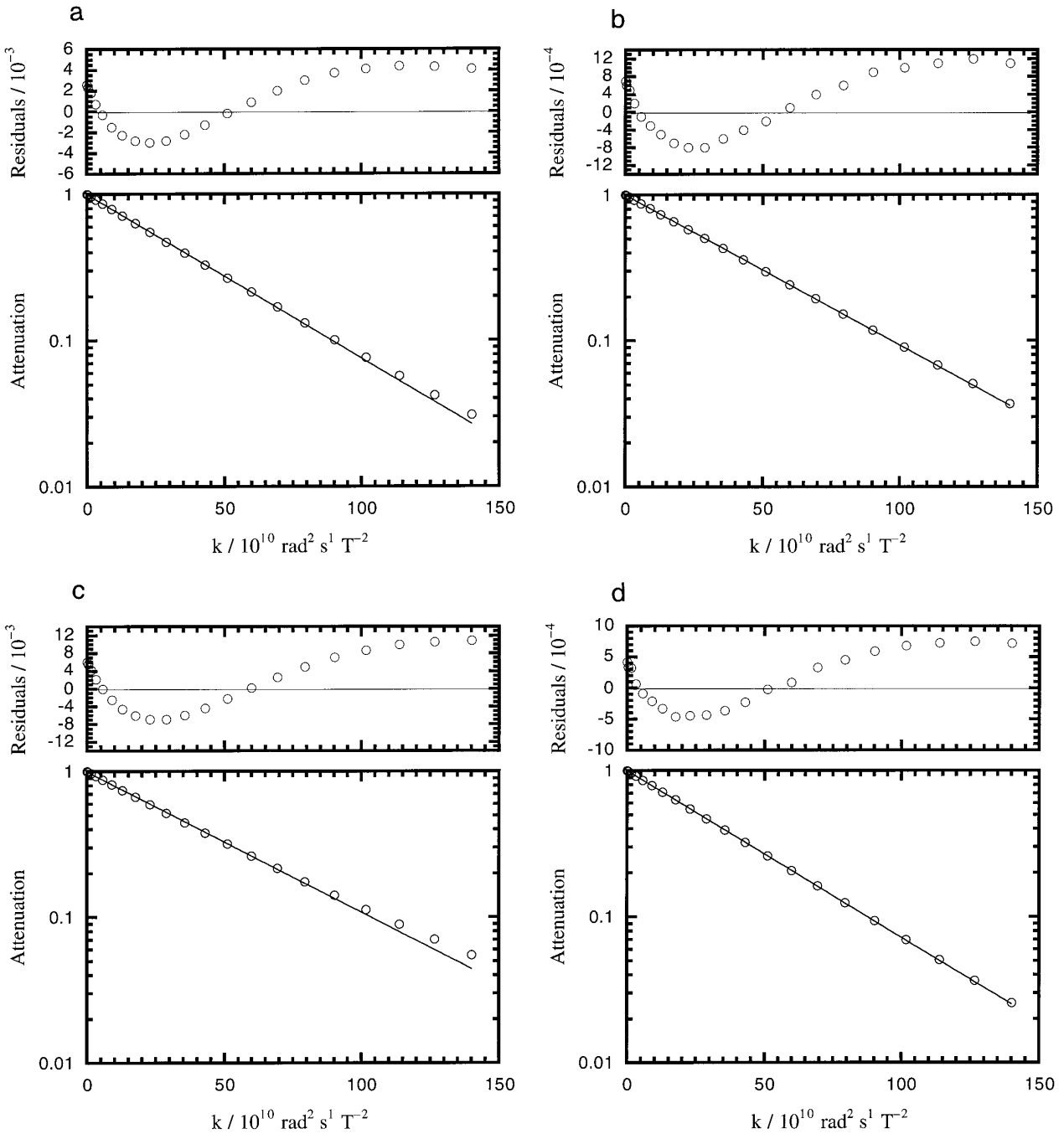


**FIG. 6.** Attenuation (○) vs $k$ [$k \equiv \gamma^2\delta^2(\Delta - \delta/3)$] from the simulations of free diffusion in the different active sample volumes: (a) A, (b) B, (c) C, and (d) D. A nonlinear least-squares fit of Eq. [1] to the data is also included (—), where $g$ (see Table 2) and the physically irrelevant parameter $E_0$ (see Eq. [1]) are optimized. The residuals (○) are included as well. Parameters used: $\Delta = 140$ ms, $D = 2 \times 10^{-9}$ m$^2$s$^{-1}$, and $B_z$ was given by Eq. [5].

tween Figs. 5 and 6 gives an indication of the error caused by using Eq. [1] in the evaluation of data from a typical gradient experiment in which the field gradient is not constant. To further validate this statement we have performed simulations for the case of a constant field gradient and for C (see Table 1) using $N = 10^6$ trajectories. The residuals in the fits of Eq. [1] to these data are presented in Fig. 7. As can be seen, the residuals for the case of a constant field gradient are now reduced (over most of the $k$ values investigated), while it remains essentially unchanged for the C case, proving that the residuals in Fig. 6 are indeed caused by the nonconstant field gradient.

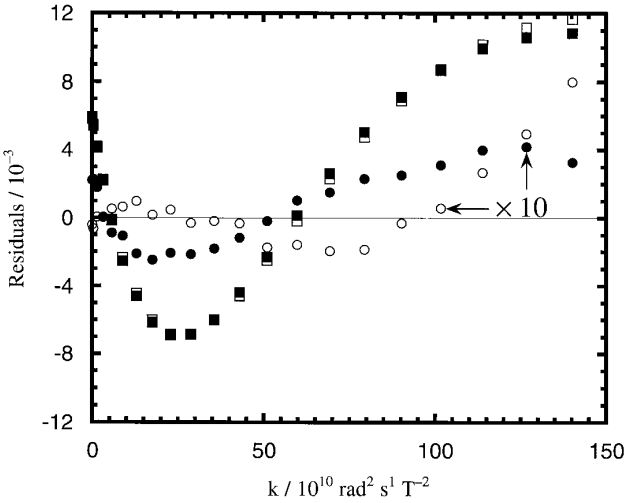


**FIG. 7.** The residuals between the simulated and the fitted attenuation vs $k$ [$k \equiv \gamma^2\delta^2(\Delta - \delta/3)$] from simulation of free diffusion with constant $g$ and $N = 10^5$ trajectories (●), constant $g$ and $N = 10^6$ trajectories (○), coil C and $N = 10^5$ trajectories (■), and coil C and $N = 10^6$ trajectories (□). Please note that the values of the residuals in the constant gradient case have been multiplied by a factor of 10. Notice also that the open squares are partly or completely hidden by the filled squares.

The results, i.e., the gradient strengths of the fits, are compiled in Table 2. By comparing the obtained values of $g$ from the fits with the calculated mean gradient (see Table 1) for each active sample volume, it is clear that there is, perhaps expected, a rather good agreement between the two values. We also note that, even when the magnetic field deviates considerably from the linear case (see Figs. 4a and 4c), the deviations in the simulated echo amplitudes compared to the linear case (see Figs. 6a and 6c) are not very pronounced.

For three of the active sample volumes (A, C, and D) we have investigated the dependence of $\Delta$, while keeping the self-diffusion coefficient constant at $D = 2 \times 10^{-9}$ m$^2$ s$^{-1}$. The fitted gradient strengths for different values of $\Delta$ are given in Table 3, and there is only a small dependence on the value of $\Delta$.

**TABLE 2**
**Results According to Fits of Eq. [1] to the Simulated Data in Fig. 6**

| Coil | $g_{fit}$ (mT m$^{-1}$) | Figure |
|---|---|---|
| A | 35.92 | 6a |
| B | 34.44 | 6b |
| C | 33.32 | 6c |
| D | 36.26 | 6d |

*Note.* Parameters used; $\Delta = 140$ ms, $D = 2 \times 10^{-9}$ m$^2$ s$^{-1}$ (close to the value of water at 25°C), and $B_z$ was given by Eq. [5].

**TABLE 3**
**Results According to Fits of Eq. [1] to Simulated Data, for Different Values of $\Delta$**

| Coil | $\Delta$ (ms) | $g_{fit}$ (mT m$^{-1}$) |
|---|---|---|
| A | 70 | 35.96 |
| | 140 | 35.92 |
| | 280 | 35.95 |
| C | 70 | 33.36 |
| | 140 | 33.32 |
| | 280 | 33.30 |
| D | 70 | 36.34 |
| | 140 | 36.26 |
| | 280 | 36.27 |

*Note.* Parameters used: $D = 2 \times 10^{-9}$ m$^2$ s$^{-1}$ (close to the value of water at 25°C) and $B_z$ was given by Eq. [5].

Moreover, we have investigated the influence of different values of the self-diffusion coefficients, while keeping the observation time constant at $\Delta = 140$ ms. The corresponding fitted gradient strengths are compiled in Table 4, and also here the simulations show very little difference for different self-diffusion coefficients.

*''Practical'' experiment.* When performing practical self-diffusion experiments, one usually follows the following protocol. First, the gradient strength $g$ is determined by performing experiments on a substance for which the self-diffusion coefficient is known [see discussion in (*3*)]. Substances often used are water (*35*) or different hydrocarbons (*36*). The gradient strength is then obtained by fitting Eq. [1] to the echo amplitudes, accumulated by different durations (or amplitudes) of the gradient pulses.

Subsequently, the PFG experiment is performed on the sample with an unknown self-diffusion coefficient $D$, and the value of $D$ is obtained by using standard fitting procedures of

**TABLE 4**
**Results According to Fits of Eq. [1] to Simulated Data, for Different Values of $D$**

| Coil | $D$ (m$^2$ s$^{-1}$) | $g_{fit}$ (mT m$^{-1}$) |
|---|---|---|
| A | $2 \times 10^{-9}$ | 35.92 |
| | $4.23 \times 10^{-10}$ | 35.93 |
| | $4 \times 10^{-11}$ | 35.92 |
| C | $2 \times 10^{-9}$ | 33.32 |
| | $4.23 \times 10^{-10}$ | 33.37 |
| | $4 \times 10^{-11}$ | 33.37 |
| D | $2 \times 10^{-9}$ | 36.26 |
| | $4.23 \times 10^{-10}$ | 36.31 |
| | $4 \times 10^{-11}$ | 36.31 |

*Note.* Parameters used: $\Delta = 140$ ms and $B_z$ was given by Eq. [5].

**TABLE 5**

**Results According to the Simulation of a ''Practical'' PFG Determination of Self-Diffusion Coefficients, Where Eq. [1] Has Been Fitted to the Simulated Data**

| Gradient calibration | | |
|---|---|---|
| Coil | $D_{act}$ ($m^2$ $s^{-1}$) | $g_{fit}$ (mT $m^{-1}$) |
| A | $4.23 \times 10^{-10}$ | 35.8 |
| D | $4.23 \times 10^{-10}$ | 36.2 |
| Determination of ''unknown'' self-diffusion coefficient | | |
| Coil | $D_{act}$ ($m^2$ $s^{-1}$) | $D_{fit}$ ($m^2$ $s^{-1}$) |
| A | $4.00 \times 10^{-11}$ | $4.03 \times 10^{-11}$ |
| D | $4.00 \times 10^{-11}$ | $4.02 \times 10^{-11}$ |

*Note.* Random noise was added to the simulated data corresponding to a *S/N* ratio of 200:1. Parameters used: $\Delta = 140$ ms and $B_z$ was given by Eq. [5]. The abbreviation ''$D_{act}$'' stands for the actual self-diffusion coefficient.

Eq. [1] (for the case of Gaussian diffusion) to the experimental data, keeping the value of $g$ constant and equal to the value from the calibration experiment.

One difference between a numerical simulation and a practical experiment is that the echo amplitudes obtained in the practical experiment will suffer from noise. To take this effect into account in the simulations, we have added noise to the simulated echo amplitudes. In our case we have used a *S/N* ratio of 200:1, which is a reasonable number in a real experiment.

In Table 5 the results of the procedure described above, for each coil design and one active sample volume (A and D), are presented. For the gradient calibration in each case, we have used hexadecane ($C_{16}H_{34}$) which has a self-diffusion coefficient of $4.23 \times 10^{-10}$ $m^2$ $s^{-1}$ at 25°C (*36*). The sample with the ''unknown'' self-diffusion coefficient has a self-diffusion coefficient of $4 \times 10^{-11}$ $m^2$ $s^{-1}$. To put this value into context, it corresponds to the self-diffusion coefficient of the surfactant in a 10 wt% aqueous solution of dodecyl octaethylene glycol ($C_{12}E_8$). The self-diffusion coefficients obtained for each coil design are in good agreement with the actual self-diffusion coefficient. The differences between the actual and the calculated values are within 1%. Please note that one of the active sample volumes corresponds to the ''worst'' case (A) of our own coil design.

To summarize this section, we note that the error introduced by the nonlinearity of the magnetic field in typical gradient coil systems introduces errors in the actually determined self-diffusion coefficients which are typically less than 1%. This is a minor effect, which is most likely masked by other sources of errors, such as temperature gradients, eddy currents, and mismatching of the gradient pulses.

## CONCLUSIONS

In conclusion, we have demonstrated that deviations from linearity in the magnetic field, as produced by the gradient system, do not influence the outcome of a PFG experiment to any significant extent. In fact, one can afford quite large deviations from linearity, as compared to those commonly found in experimental setups, without losing too much accuracy in the self-diffusion coefficient obtained. As a consequence, it is recommended that the radius of the main gradient coil be decreased, although this produces a poorer linearity of the magnetic field. The advantages are, however, higher gradient strengths and a reduced far field. Large values of the far field may cause problems such as eddy currents, which deteriorate the quality of the experiments.

The Brownian-dynamics computer simulation procedure presented here offers a quantitative way of investigating the performance characteristics of a gradient coil of a certain design before it is built.

## ACKNOWLEDGMENT

This work was financially supported by the Swedish Natural Science Research Council.

## REFERENCES

1. P. T. Callaghan, *Aust. J. Phys.* **37,** 359 (1984).
2. P. Stilbs, *Prog. NMR Spectrosc.* **19,** 1 (1987).
3. O. Söderman and P. Stilbs, *Prog. NMR Spectrosc.* **26,** 445 (1994).
4. B. Lindman, O. Söderman, and H. Wennerström, *Surf. Sol.: New Methods Invest.* **22,** 295 (1987).
5. B. Lindman, K. Shinoda, U. Olsson, D. Anderson, G. Karlström, and H. Wennerström, *Colloids Surf.* **38,** 205 (1989).
6. B. Balinov, U. Olsson, and O. Söderman, *J. Phys. Chem.* **95,** 5931 (1991).
7. P. Ström and D. Anderson, *Langmuir* **8,** 691 (1992).
8. P. T. Callaghan, A. Coy, D. MacGowan, K. J. Packer, and F. O. Zelaya, *Nature* **351,** 467 (1991).
9. P. T. Callaghan, A. Coy, T. P. J. Halpin, D. MacGowan, K. J. Packer, and F. O. Zelaya, *J. Chem. Phys.* **97,** 651 (1992).
10. P. Becher, ''Encyclopedia of Emulsion Technology. Basic Theory Measurement Applications,'' Dekker, New York/Basel, 1988.
11. K. Packer and C. Rees, *J. Colloid Interface Sci.* **40,** 206 (1971).
12. P. T. Callaghan, R. Humphrey, and K. W. Jolley, *J. Colloid Interface Sci.* **93,** 521 (1983).
13. I. Lönnqvist, A. Khan, and O. Söderman, *J. Colloid Interface Sci.* **144,** 401 (1991).
14. O. Söderman, I. Lönnqvist, and B. Balinov, *in* ''Emulsions—A Fundamental and Practical Approach'' (J. Sjöblom, Ed.), Kluwer, Amsterdam, 1992.
15. J. E. Tanner, *Rev. Sci. Instrum.* **36,** 1086 (1965).
16. J. E. Tanner, Thesis, University of Wisconsin, 1966.
17. D. S. Webster and K. H. Marsden, *Rev. Sci. Instrum.* **45,** 1232 (1974).

*18.* G. Ödberg and L. Ödberg, *J. Magn. Reson.* **16,** 342 (1974).
*19.* R. F. Karlicek and I. J. Lowe, *J. Magn. Reson.* **37,** 75 (1980).
*20.* I. Zupancic and J. Pirs, *J. Phys. E: Sci. Instrum.* **9,** 79 (1976).
*21.* W. T. Sobol and J. S. Blicharski, *J. Magn. Reson.* **60,** 83 (1984).
*22.* M. A. Martens, L. S. Petropoulos, R. W. Brown, J. A. Andrews, M. A. Morich, and J. L. Patrick, *Rev. Sci. Instrum.* **62,** 2639 (1991).
*23.* M. I. Hrovat and C. G. Wade, *J. Magn. Reson.* **45,** 67 (1981).
*24.* E. von Meerwall and M. Kamat, *J. Magn. Reson.* **83,** 309 (1989).
*25.* P. Mansfield and B. Chapman, *J. Magn. Reson.* **66,** 573 (1986).
*26.* P. Mansfield and B. Chapman, *J. Phys. E: Sci. Instrum.* **19,** 540 (1986).
*27.* P. B. Roemer, W. A. Edelstein, and J. S. Hickey, Abstracts of the Society Magnetic Resonance in Medicine, 5th Annual Meeting, Montreal, 1986.
*28.* A. Jasinski, T. Jakubowski, M. Rydzy, P. Morris, I. C. P. Smith, P. Kozlowski, and J. K. Saunders, *Magn. Reson. Med.* **24,** 29 (1992).
*29.* S. J. Gibbs, K. F. Morris, and C. S. Johnson, Jr., *J. Magn. Reson.* **94,** 165 (1991).
*30.* E. O. Stejskal and J. E. Tanner, *J. Chem. Phys.* **42,** 288 (1965).
*31.* J. D. Jackson, ''Classical Electrodynamics,'' Wiley, New York/London/Sydney, 1962.
*32.* M. Abramowitz and I. A. Stegun, ''Handbook of Mathematical Functions,'' Dover, New York, 1965.
*33.* D. L. Ermak and Y. Yeh, *Chem. Phys. Lett.* **24,** 243 (1974).
*34.* D. L. Ermak, *J. Chem. Phys.* **62,** 4189 (1975).
*35.* R. Mills, *J. Phys. Chem.* **77,** 685 (1973).
*36.* H. Ertl and F. A. L. Dullien, *AIChE J.* **19,** 1215 (1973).